Angle-resolved Rabi flopping in strong-field dissociation of molecules

Chen-Xi Hu,[1] Wei-Zhe Li,[2] Wen-Bin Zhang,[3] Xiao-Chun Gong,[3] Jian Wu,[3,4,5,*] and Feng He[1,5,†]

[1]*Key Laboratory for Laser Plasmas (Ministry of Education) and School of Physics and Astronomy, Collaborative Innovation Center of IFSA (CICIFSA), Shanghai Jiao Tong University, Shanghai 200240, China*

[2]*Zhiyuan College, Shanghai Jiao Tong University, Shanghai 200240, China*

[3]*State Key Laboratory of Precision Spectroscopy, East China Normal University, Shanghai 200062, China*

[4]*Collaborative Innovation Center of Extreme Optics, Shanxi University, Taiyuan, Shanxi 030006, China*

[5]*CAS Center for Excellence in Ultra-intense Laser Science, Shanghai 201800, China*

(Received 10 April 2020; revised 24 February 2021; accepted 15 April 2021; published 29 April 2021)

Rabi flopping is a paradigm of two-level quantum systems in the presence of an oscillatory driving field. Different from atoms, the Rabi flopping in a molecule depends on its bond length and orientation with respect to the light polarization direction. Here we explore the Rabi flopping in the strong-field dissociation of H_2^+ in which the two lowest electronic states are photon coupled. H_2^+ aligned along different angles experiences different laser intensities, building the Rabi flopping with angle-dependent frequencies. During the laser-H_2^+ interaction, the electron completes different fractions of Rabi flopping for H_2^+ aligned in different directions, leading to the angular nodes and maxima in the dissociative proton momentum distribution. Our study reveals that one-photon dissociation undergoes the alternation of absorbing and emitting one photon, instead of the one-off photon absorption. This study also provides a universal explanation for the angular distribution of the dissociative fragments in strong laser fields.

DOI: 10.1103/PhysRevA.103.043122

I. INTRODUCTION

The exposure of a two-level quantum system to an oscillatory driving field leads to the formation of Rabi flopping [1], which plays a significant role almost everywhere, such as building the architecture of quantum computation [2], controlling the state of a single quantum dot spin [3], reshaping the transmitted light pulses in atoms [4], and realizing the quantum circuit in a superconducting resonator [5]. With the advent of ultrashort laser pulses, one is able to watch in real time the ultrafast Rabi oscillations [6] between excitons and plasmons or reconstruct the full temporal dipole response in atoms [7]. While Rabi flopping is a paradigm in light-matter interaction, surprisingly, it has not been extensively discussed in molecular dissociation.

As the simplest molecule, H_2^+ offers a perfect platform to study the ultrafast correlation between electrons and nuclei and has attracted a great deal of attention in past decades [8,9]. The dissociation of H_2^+ has been extensively studied, and a series of dissociation pathways has been explored, such as zero-photon [10], one-photon [11,12], three-photon [13,14], net-two-photon [15], and rescattering-assisted [16,17] dissociation. Different dissociation pathways can be well recognized by coincidentally measuring the ejected electron and nuclear fragments [18]. The dissociation dynamics of H_2^+ is mostly determined by laser coupling between the two lowest electronic states, i.e., the $1s\sigma_g$ and $2p\sigma_u$ states. We expect to observe the Rabi flopping in such a very neat two-level system.

In this paper we study the dissociation of H_2^+ in a linearly polarized few-cycle laser pulse and explore the angle-resolved Rabi flopping. The Rabi flopping significantly modifies the angular distribution of the dissociative fragments. The proton angular distribution after the dissociation of H_2^+ has been investigated in the past two decades. It is believed that the transition amplitude between the $1s\sigma_g$ and $2p\sigma_u$ states is proportional to $\mathbf{D}(\mathbf{R}) \cdot \mathbf{E}(t)$, where $\mathbf{D}(\mathbf{R})$ is the dipole, $\mathbf{R}$ is the internuclear displacement, and $\mathbf{E}(t)$ is the driving laser field. Hence, for a linearly polarized driving laser pulse, it is intuitive that the coupling is strongest if the direction of $\mathbf{D}(\mathbf{R})$ is parallel to the direction of $\mathbf{E}(t)$. Several experiments [19–24] measured proton angular distributions and found that proton angular distributions can be approximately fitted by $\cos^{2n}\theta$, with n an integer and θ the crossing angle between the molecular axis and the laser polarization direction. Though the exactly angular distribution depends on the dissociation pathway, kinetic energy release (KER), and laser intensity, one common characteristic is that the angular probability peaks at $\theta = 0$ and gradually decreases with an increase of θ from 0 to $\pi/2$. However, our study shows that the dissociative proton momentum distribution presents multiple angular nodes and maxima, which are determined by the θ-dependent Rabi flopping between the $1s\sigma_g$ and $2p\sigma_u$ states. It is the focal-volume intensity average in experiments that smears out the angular structures and results in the $\cos^{2n}\theta$ distribution.

*jwu@phy.ecnu.edu.cn
†fhe@sjtu.edu.cn

II. NUMERICAL METHODS AND RESULTS

The dissociation of H_2^+ in strong laser fields is governed by the time-dependent Schrödinger equation (TDSE) (atomic units $e = \hbar = m = 1$ are used throughout unless otherwise stated)

$$i\frac{\partial}{\partial t}\psi_\theta(x,y,R;t) = \left[\frac{P_R^2}{2M} + \frac{p_y^2}{2} + \frac{p_x^2}{2} + \frac{1}{R} + xE(t) - \frac{1}{\sqrt{\left(x-\frac{R}{2}\sin\theta\right)^2 + \left(y-\frac{R}{2}\cos\theta\right)^2 + \left(\frac{\beta(R)}{5}\right)^2} + \frac{1}{\beta(R)} - \frac{\beta(R)}{5}} - \frac{1}{\sqrt{\left(x+\frac{R}{2}\sin\theta\right)^2 + \left(y+\frac{R}{2}\cos\theta\right)^2 + \left(\frac{\beta(R)}{5}\right)^2} + \frac{1}{\beta(R)} - \frac{\beta(R)}{5}}\right]\psi_\theta(x,y,R;t). \quad (1)$$

Here the electron dynamics is confined in the (x, y) plane. The molecular axis is placed within this plane and the nuclear dynamics is confined along the molecular axis. The crossing angle θ between the molecular axis and the x axis in the model is a parameter instead of a dynamical variable and thus the molecular rotation is not allowed. In addition, $M = 918$ a.u. is the reduced nuclear mass, P_R is the nuclear momentum operator along the molecular axis, and p_x and p_y are electron momentum operators along the x and y directions, respectively. We introduce the R-dependent soft-core parameter $\beta(R)$ in order to ensure that the $1s\sigma_g$ and $2p\sigma_u$ potential curves in this model are good enough [25]. In the later simulation using this model, the initial state is the superposition of first ten vibrational states weighted by Frank-Condon coefficients and each vibrational state is numerically obtained by using the imaginary-time propagation algorithm [26]. The Crank-Nicolson method [27] is adopted to propagate the nuclear wave packet in real time. Since we focus on the dissociation, the ionized wave packets in the calculations are absorbed by setting a mask function in numerical boundaries. The spatial axes x, y, and R span the areas $[-30, 30]$, $[-30, 30]$, and $[0, 16]$ a.u., respectively. The spatial steps are $dx = dy = 0.2$ a.u. and $dR = 0.02$ a.u. and the time step is $dt = 0.1$ a.u. The KER of the dissociative fragments is obtained by Fourier transforming the dissociative molecular wave packet after it enters the area $R > 10$ and has clearly separated from bound states. By scanning θ, the nuclear momentum distribution in the two-dimensional plane $(P_{Rx}, P_{Ry}) = (P_R\cos\theta, P_R\sin\theta)$ is formed. The convergence of the simulations has been approved by using smaller spatial-time steps. The free propagation of the initial state gives rise to the molecular bond vibration, followed by wave function collapse and revival in the $1s\sigma_g$ potential curve [28]. We propagate the nuclear wave packet for $\Delta t = 8$ fs before the following laser pulse is introduced:

$$\mathbf{E}(t) = E_0\cos[\omega(t-\Delta t)]\sin^2\left[\pi\frac{t-\Delta t}{\tau}\right]\mathbf{e}_x, \quad \Delta t < t < \tau + \Delta t. \quad (2)$$

Here ω is the laser frequency, E_0 is the electric amplitude, and τ is the pulse width. In addition, $\mathbf{e}_x$ is the unit vector and the laser pulse is always polarized along the x axis. For H_2^+, the free propagation of 8 fs leads to the nuclear wave packet mainly being distributed in the area 3 a.u. $< R <$ 8 a.u., assisting the one-photon transition but suppressing the three-photon transition between the $1s\sigma_g$ and $2p\sigma_u$ states by the forthcoming laser pulse, since the one- and three-photon transitions mainly happen at $R = 3.8$ and 2.3 a.u., respectively, if the driving laser wavelength is 400 nm. Figures 1(a) and 1(b) present the nuclear momentum distributions when the laser wavelengths are 400 and 800 nm, respectively. Other parameters are given in the caption. One may clearly see that multiple nodes and maxima appear at different angles. The $\cos^2\theta$ distribution law is completely broken. The calculated ionization probability is less than 1%.

It is hard for the above *ab initio* calculations to illustrate clearly the physical mechanism. In order to get an intuitive understanding, we compare the above results with the two-level model below. Since in most cases the dynamics of H_2^+ dissociation is confined within the $1s\sigma_g$ and $2p\sigma_u$ states, we

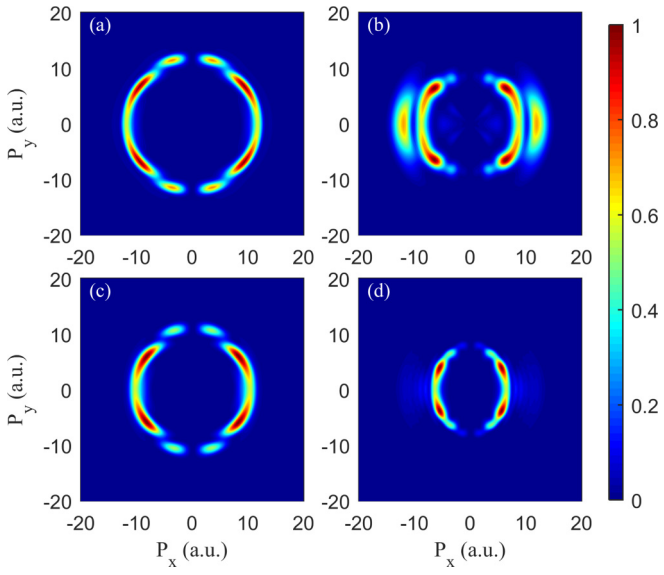

FIG. 1. Proton momentum distributions calculated by (a) and (b) the full TDSE model and (c) and (d) the two-level model for (a) and (c) laser wavelength 400 nm, intensity 5×10^{13} W/cm^2, and duration of six optical cycles (8 fs) and (b) and (d) laser wavelength 800 nm, intensity 6×10^{13} W/cm^2, and duration of four optical cycles (10.7 fs). The distributions are normalized by their own maxima in each panel.

thus use the simplified two-level model

$$i\frac{\partial}{\partial t}\begin{pmatrix}\chi_g(\mathbf{R},t)\\ \chi_u(\mathbf{R},t)\end{pmatrix} = \begin{pmatrix}\frac{\mathbf{P}_\mathbf{R}^2}{2M}+V_g(\mathbf{R}) & \mathbf{D}(\mathbf{R})\cdot\mathbf{E}(t)\\ \mathbf{D}(\mathbf{R})\cdot\mathbf{E}(t) & \frac{\mathbf{P}_\mathbf{R}^2}{2M}+V_u(\mathbf{R})\end{pmatrix}\begin{pmatrix}\chi_g(\mathbf{R},t)\\ \chi_u(\mathbf{R},t)\end{pmatrix}. \quad (3)$$

Now $\mathbf{R}$ is confined in a two-dimensional plane constructed by the molecular axis and laser polarization direction, and the molecular rotation is now allowed. Here $V_g(\mathbf{R})$ and $V_u(\mathbf{R})$ are the potential surfaces for $H_2{}^+$ in the $1s\sigma_g$ and $2p\sigma_u$ states, respectively [29]; $\chi_g(\mathbf{R},t)$ and $\chi_u(\mathbf{R},t)$ are the nuclear wave packets associated with the electron in the $1s\sigma_g$ and $2p\sigma_u$ states, respectively. The spatial-time steps are $dR_x = dR_y = 0.02$ and $dt = 0.1$ a.u.; R_x and R_y span the area $0 < R_x < 30$ and $0 < R_y < 30$. The two-dimensional simulation box is big enough to hold all dissociative wave packets during the interaction and thereby no absorbing boundary conditions are used. Initially, $\chi_u(\mathbf{R}, t=0) = 0$ and $\chi_g(\mathbf{R}, t=0) = \chi_{H_2}$, with χ_{H_2} the nuclear ground state of H_2 with an isotopic distribution in space. Strictly speaking, the single ionization of H_2 depends on the orientation of the molecular axis with respect to the laser polarization. However, the initially anisotropic nuclear wave-packet distribution of $H_2{}^+$ does not noticeably modify the Rabi flopping, which is mainly determined by the relative populations of $1s\sigma_g$ and $2p\sigma_u$ states. Figures 1(c) and 1(d) show the nuclear momentum distributions, where the laser parameters are the same as those used in Figs. 1(a) and 1(b), respectively. The two models give very similar simulation results, especially for the location of angular nodes and maxima. The small discrepancies are due to the slightly different $2p\sigma_u$ potential curves in the two models. The dissociation probabilities are around 10%. The similarity of the two rows in Fig. 1 indicates that the molecular rotation, higher electronic states, and ionization do not play noticeable roles for the observed multiple nodes and maxima in the nuclear momentum distribution. The main dynamics is solely governed by the photon-couple dipole transition between the $1s\sigma_g$ and $2p\sigma_u$ states. The Stark shift and Raman scattering are included in the two models, but do not govern the dynamics.

Since the two-level model already describes the dissociation correctly, we analyze the dynamics based on the two-level model in the following. By tracing the nuclear wave-packet propagation, we learn that all dissociative fragments in Figs. 1(c) and 1(d) dissociate along the $2p\sigma_u$ state and the ultimate KER peaks at 1.5 eV in Fig. 1(c) and at 0.7 eV in Fig. 1(d). Thereby, we conclude that $H_2{}^+$ dissociates via the one-photon (bond softening) pathway, though the angular distribution is far away from the $\cos^{2n}\theta$ distribution. Figures 2(a) and 2(b) show the time-evolved angular distribution of $|\chi_u(\mathbf{R},t)|^2$. A movie of the nuclear wave-packet propagation on the $2p\sigma_u$ state can be found in the Supplemental Material [30] (the laser parameters are shown in the caption of Fig. 2). For the calculation of Fig. 2(a), the 400-nm laser field turns on at $t = 8$ fs and vanishes at $t = 16$ fs. During this interaction, the probability of the $2p\sigma_u$ state fluctuates significantly, indicating that the electron is transiting between $1s\sigma_g$ and $2p\sigma_u$ states. The population on the $2p\sigma_u$ state reaches

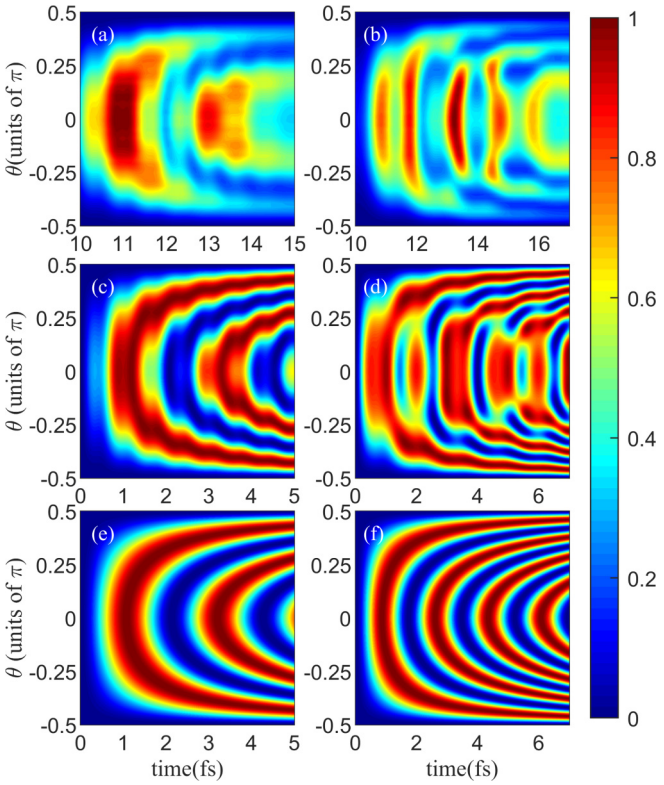

FIG. 2. Time-evolved angular distribution $\chi_u(\mathbf{R},t)$, calculated by (a) and (b) the two-level model, (c) and (d) the simpler two-level model by assuming transitions solely happen at R_r without using the rotating-wave approximation, and (e) and (f) the rotating-wave approximation for (a), (c), and (e) laser wavelength 400 nm, intensity 5×10^{13} W/cm^2, and duration 8 fs and (b), (d), and (f) laser wavelength 800 nm, intensity 6×10^{13} W/cm^2, and duration 10.7 fs. The distributions are normalized by their own maxima in each panel.

the maximum at $t = 11$ fs; however, this part is not necessary to dissociate because it might dump to the $1s\sigma_g$ state and stay bound. The alternation of absorbing and emitting one photon [31] and swapping the probabilities of two states are the typical Rabi flopping in two-level systems. The Rabi frequency $\omega_r = \sqrt{[V_u(\mathbf{R}) - V_g(\mathbf{R}) - \omega]^2 + [E_0 D(\mathbf{R})\cos\theta]^2}$ depends on the crossing angle θ between $\mathbf{D}(\mathbf{R})$ and $\mathbf{E}(t)$. For example, in Fig. 2(a), at $\theta = 0$, two full Rabi oscillations are formed within the laser pulse duration and thus $H_2{}^+$ returns to the $1s\sigma_g$ state, leading to a local minimum in the dissociative fragment momentum distribution. However, at $\theta = \pm 0.2\pi$, the molecule experiences a weaker laser intensity and thus the molecule finishes 1.5 Rabi oscillations, ending on the $2p\sigma_u$ state and creating a local maximum in the angular distribution. At $\theta = \pm 0.4\pi$, the molecule experiences a very weak laser intensity (about 10% of the peak intensity I_0) and no Rabi flopping is formed. Besides the Rabi flopping, another faint flopping with the frequency $2\omega_{400}$ is also presented in Fig. 1(a). Such a $2\omega_{400}$ flopping has few contributions to the ultimate angular distribution and is generally filtered out under the rotating-wave approximation, to be discussed below. A similar scenario happens in Fig. 2(b); however, the $2\omega_{800}$ frequency is close to the Rabi frequency and the

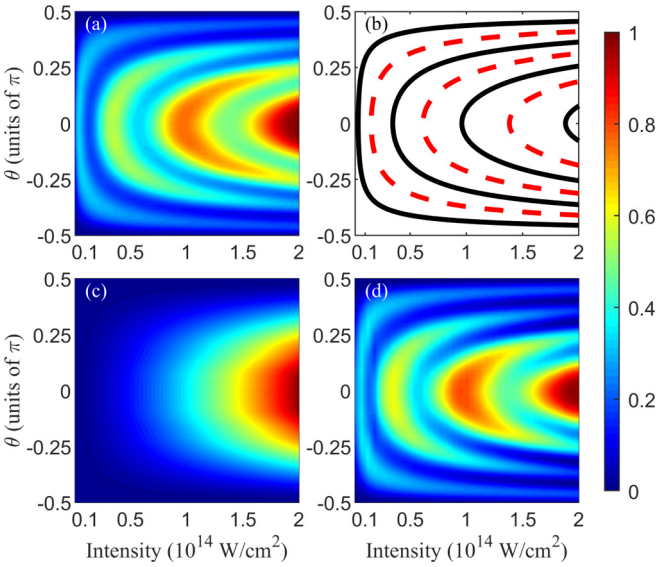

FIG. 3. (a) Proton momentum angular distribution as a function of the laser intensity. (b) Maxima (black solid curves) and minima (red dashed curves) formulated by $I\cos^2\theta = \text{const}$ detailed in the text. (c) Focal-volume intensity-averaged proton momentum angular distribution as a function of the laser peak intensity. (d) Proton momentum angular distribution driven by uniform laser intensities, extracted from the intensity-integrated data in (a). The laser wavelength is 400 nm and the pulse comprises six optical cycles. The distributions are normalized by their own maxima in (a), (c), and (d).

mixture of these two frequencies blurs the distinct Rabi flopping.

Assuming that the Rabi flopping is driven by a plane wave and it mainly occurs at the internuclear distance R_r where $V_u(R_r) - V_g(R_r) = \omega$, we calculate the time-dependent angular distributions in the $2p\sigma_u$ state and show them in Figs. 2(c) and 2(d). Furthermore, if the rotating-wave approximation is adopted, the time-dependent angular population in the $2p\sigma_u$ state can be analytically formulated as [32]

$$P_u(\theta, t) = \sin^2\left(\frac{E_0 D(R_r)\cos\theta}{2}t\right), \tag{4}$$

as shown in Figs. 2(e) and 2(f). The rotating-wave approximation eliminates the 2ω flopping in Figs. 2(c) and 2(d). Such a very simple analytical formula reproduces the overall structures in Figs. 2(a) and 2(b) very well, which gives a solid confirmation that the angular nodes and maxima are indeed induced by Rabi flopping. Note that in the derivation of Eq. (4), a continuously electric field is assumed. Using the laser field expressed by Eq. (2) in the Rabi flopping model, better agreement with the numerical simulation results can be achieved.

Since the Rabi frequency depends on the laser intensity, one may expect that the angular distribution should also depend on the laser intensity. By scanning the laser intensity between 1×10^{12} and 2×10^{14} W/cm^2, we show the angle-resolved dissociation probability as a function of the laser intensity in Fig. 3(a). It is clear that the momentum angular distribution can be fitted by $\cos^2\theta$ if the laser field is too weak to initiate the Rabi flopping. However, when the laser intensity is higher than 10^{13} W/cm^2, which is a modest intensity in many experiments, distinct Rabi flopping determines the angular distribution of the dissociative fragments. According to Eq. (4), the angle-dependent dissociation probability approaches maximum when $\frac{E_0 D(R_r)\cos\theta}{2}t = (n - \frac{1}{2})\pi$, with n an integer starting from 1. Therefore, after the interaction with the laser field, the locations of maxima in Fig. 3(a) can be fitted by $I\cos^2\theta = [\frac{(n-1/2)\pi}{D(R_r)\tau}]^2$, in which we have assumed the transition happens at R_r and $t = \tau/2$, i.e., only the central half-width of the laser pulse is strong enough to trigger the Rabi flopping. On the contrary, the minima are located at $I\cos^2\theta = [\frac{n\pi}{D(R_r)\tau}]^2$. The maxima and minima of the angle-resolved dissociation probability are shown by black solid and red dashed curves in Fig. 3(b). Actually, the curves $I\cos^2\theta = \text{const}$ mark the effective laser intensity experienced by the molecule aligned along θ. On the three black solid curves, H_2^+ undergoes $\frac{1}{2}$, $\frac{3}{2}$, and $\frac{5}{2}$ Rabi oscillations and thus the population on the $2p\sigma_u$ state and the dissociation probability reach maxima. On the contrary, the angle-resolved dissociation probability reaches a minimum when full Rabi flopping is accomplished.

The dependence on intensity implies that the angular nodes and maxima could be smeared out by the focal-volume intensity average in experiment. Assuming H_2^+ is dissociated by a focused Gaussian laser beam having the spatial-intensity distribution $V(I)$ [33], to get the final momentum distribution, one should integrate the dissociative fragments in Fig. 3(a) weighted by a factor $f(I_0, I_{0m})$, which is the volume proportion of a certain intensity I_{0m} when the peak intensity is I_0, i.e.,

$$W(P_x, P_y; I_0) = \sum_m |\tilde{\chi}_u(P_x, P_y; I_{0m})|^2 f(I_0, I_{0m}), \tag{5}$$

where $\tilde{\chi}_u$ is the dissociative nuclear wave packet in momentum representation and m is the index marking the intensity ingredients in the focused pulse. Incidentally, if the single ionization of H_2 and the later dissociation of H_2^+ are driven by the same pulse, the tunneling ionization rate of H_2 should be incorporated into $f(I_0, I_{0m})$. After doing the focal-volume intensity average, we show the proton angular distribution in Fig. 3(c), where the nodes disappear and the probability peaks at $\theta = 0$. We thereby conjecture that the Rabi flopping has already happened in many experiments; however, the unavoidable focal-volume intensity average in experiments may prohibit the direct observation of multiple nodes and maxima.

To experimentally observe the multiple angular nodes and maxima, one is required to extract the dissociative fragments driven by a uniform laser intensity from the intensity-integrated momentum angular distribution. We develop here an algorithm to extract the uniform-intensity triggered dissociative fragments. Provided a series of experiments with the peak intensity I_{0m} has been performed and the intensity-integrated proton momentum distributions $W(P_x, P_y; I_{0m})$ are

measured, one may write the matrix

$$\begin{pmatrix} W(P_x, P_y; I_{01}) \\ W(P_x, P_y; I_{02}) \\ W(P_x, P_y; I_{03}) \\ \vdots \\ W(P_x, P_y; I_{0m}) \end{pmatrix} = \mathbf{T} \begin{pmatrix} |\tilde{\chi}_u(P_x, P_y; I_{01})|^2 \\ |\tilde{\chi}_u(P_x, P_y; I_{02})|^2 \\ |\tilde{\chi}_u(P_x, P_y; I_{03})|^2 \\ \vdots \\ |\tilde{\chi}_u(P_x, P_y; I_{0m})|^2 \end{pmatrix}, \tag{6}$$

where the matrix T is written as

$$\mathbf{T} = \begin{pmatrix} f(I_{01}, I_{01}) & f(I_{01}, I_{02}) & f(I_{01}, I_{03}) & \cdots & f(I_{01}, I_{0m}) \\ 0 & f(I_{02}, I_{02}) & f(I_{02}, I_{03}) & \cdots & f(I_{02}, I_{0m}) \\ 0 & 0 & f(I_{03}, I_{03}) & \cdots & f(I_{03}, I_{0m}) \\ \vdots & \vdots & \vdots & \ddots & \vdots \\ 0 & 0 & 0 & \cdots & f(I_{0m}, I_{0m}) \end{pmatrix}. \tag{7}$$

Note that $I_{01} > I_{02} > \cdots > I_{0m}$. By multiplying T^{-1} from the left side, $|\tilde{\chi}_u(P_x, P_y; I_{0m})|^2$ is obtained. Figure 3(d) shows the extracted $|\tilde{\chi}_u(P_x, P_y; I_{0m})|^2$ by assuming that 40 experiments are performed with the highest peak intensity $I_{01} = 2 \times 10^{14}$ W/cm^2 and the lowest peak intensity $I_{040} = 0.01 \times 10^{14}$ W/cm^2. One may clearly see that the Rabi-flopping-determined structures can be extracted. More simulations show that if the laser intensity has an uncertainty no more than 5×10^{12} W/cm^2, one may still extract the Rabi flopping using the above algorithm.

Experimentally, in contrast, if one ionizes H_2 using an isolated attosecond pulse and controls the Rabi flopping by a time-delayed femtosecond pulse, the focal-volume intensity average can be avoided since the tiny focal spot of the attosecond pulse can be located in the center spot of the femtosecond pulse focal volume. Another advantage of using such an attosecond pump pulse is that a spatially localized nuclear wave packet produced in the ionization step will be streaked by the femtosecond pulse uniformly.

In this study, it is the integration of the Rabi flopping that determines the final proton momentum distribution. If the two levels participating in Rabi flopping have significantly different energies, the Rabi flopping can be viewed in real time by introducing an extra attosecond pulse to ionize the target, since the upper and lower states have different ionization rates. The time-resolved Rabi flopping may be mapped onto the time-dependent ionization rate. We would also like to point out that the Rabi flopping is fundamentally different from the mechanism of light-induced conical intersection [34,35], since the molecular rotation is not involved in this study.

III. CONCLUSIONS

To conclude, we have explored the Rabi flopping in the one-photon dissociation. For molecules aligned along different directions, they experience different effective laser intensities, leading to angle-dependent Rabi flopping between the $1s\sigma_g$ and $2p\sigma_u$ states. When the laser pulse is turned off, H_2^+ aligned in different directions may stay either in the $2p\sigma_u$ states, followed by the dissociation, or in the $1s\sigma_g$ state, ending with the bound H_2^+. The well-known $\cos^2\theta$ distribution is actually generated by the incoherent summation of all dissociative fragments driven by different intensities in the pulse. To experimentally observe this angular structure, an attosecond-pump and UV- or infrared-probe strategy is suggested.

ACKNOWLEDGMENTS

This work was supported by National Key R&D Program of China (Grants No. 2018YFA0404802 and No. 2018YFA0306303), Innovation Program of Shanghai Municipal Education Commission (Grant No. 2017-01-07-00-02-E00034), National Natural Science Foundation of China (Grants No. 11574205, No. 11721091, No. 91850203, No. 11761141004, No. 11834004, and No. 11704124,), and Shanghai Shuguang Project (No. 17SG10). Simulations were performed on the π supercomputer at Shanghai Jiao Tong University.

[1] I. I. Rabi, Phys. Rev. **49**, 324 (1936).
[2] A. Blais, R.-S. Huang, A. Wallraff, S. M. Girvin, and R. J. Schoelkopf, Phys. Rev. A **69**, 062320 (2004).
[3] D. Press, T. D. Ladd, B. Zhang, and Y. Yamamoto, Nature (London) **456**, 218 (2008).
[4] G. B. Hocker and C. L. Tang, Phys. Rev. Lett. **21**, 591 (1968).
[5] Y. Kubo, F. R. Ong, P. Bertet, D. Vion, V. Jacques, D. Zheng, A. Dréau, J.-F. Roch, A. Auffeves, F. Jelezko, J. Wrachtrup, M. F. Barthe, P. Bergonzo, and D. Esteve, Phys. Rev. Lett. **105**, 140502 (2010).
[6] P. Vasa, W. Wang, R. Pomraenke, M. Lammers, M. Maiuri, C. Manzoni, G. Cerullo, and C. Lienau, Nat. Photon. **7**, 128 (2013).

[7] V. Stooß, S. M. Cavaletto, S. Donsa, A. Blättermann, P. Birk, C. H. Keitel, I. Březinová, J. Burgdörfer, C. Ott, and T. Pfeifer, Phys. Rev. Lett. **121**, 173005 (2018).

[8] A. Giusti-Suzor, F. H. Mies, L. F. DiMauro, E. Charron, and B. Yang, J. Phys. B **28**, 309 (1995).

[9] H. Ibrahim, C. Lefebvre, A. D. Bandrauk, A. Staudte, and F. Légaré, J. Phys. B **51**, 042002 (2018).

[10] J. H. Posthumus, J. Plumridge, L. J. Frasinski, K. Codling, E. J. Divall, A. J. Langley, and P. F. Taday, J. Phys. B **33**, L563 (2000).

[11] A. D. Bandrauk and M. L. Sink, J. Chem. Phys. **74**, 1110 (1981).

[12] P. H. Bucksbaum, A. Zavriyev, H. G. Muller, and D. W. Schumacher, Phys. Rev. Lett. **64**, 1883 (1990).

[13] A. Giusti-Suzor and F. H. Mies, Phys. Rev. Lett. **68**, 3869 (1992).

[14] J. McKenna, F. Anis, A. M. Sayler, B. Gaire, N. G. Johnson, E. Parke, K. D. Carnes, B. D. Esry, and I. Ben-Itzhak, Phys. Rev. A **85**, 023405 (2012).

[15] A. Giusti-Suzor, X. He, O. Atabek, and F. H. Mies, Phys. Rev. Lett. **64**, 515 (1990).

[16] M. F. Kling, C. Siedschlag, A. J. Verhoef, J. I. Khan, M. Schultze, T. Uphues, Y. Ni, M. Uiberacker, M. Drescher, F. Krausz, and M. J. J. Vrakking, Science **312**, 246 (2006).

[17] P. Lu, J. Wang, H. Li, K. Lin, X. Gong, Q. Song, Q. Ji, W. Zhang, J. Ma, H. Li, H. Zeng, F. He, and J. Wu, Proc. Natl. Acad. Sci. USA **115**, 2049 (2018).

[18] P. Lu, W. Zhang, X. Gong, Q. Song, K. Lin, Q. Ji, J. Ma, F. He, H. Zeng, and J. Wu, Phys. Rev. A **95**, 033404 (2017).

[19] I. D. Williams, P. McKenna, B. Srigengan, I. M. G. Johnston, W. A. Bryan, J. H. Sanderson, A. El-Zein, T. R. J. Goodworth, W. R. Newell, P. F. Taday, and A. J. Langley, J. Phys. B **33**, 2743 (2000).

[20] K. Sändig, H. Figger, and T. W. Hänsch, Phys. Rev. Lett. **85**, 4876 (2000).

[21] P. Q. Wang, A. M. Sayler, K. D. Carnes, J. F. Xia, M. A. Smith, B. D. Esry, and I. Ben-Itzhak, J. Phys. B **38**, L251 (2005).

[22] J. McKenna, A. M. Sayler, F. Anis, B. Gaire, N. G. Johnson, E. Parke, J. J. Hua, H. Mashiko, C. M. Nakamura, E. Moon, Z. Chang, K. D. Carnes, B. D. Esry, and I. Ben-Itzhak, Phys. Rev. Lett. **100**, 133001 (2008).

[23] X. Gong, P. He, Q. Song, Q. Ji, H. Pan, J. Ding, F. He, H. Zeng, and J. Wu, Phys. Rev. Lett. **113**, 203001 (2014).

[24] A. Natan, M. R. Ware, V. S. Prabhudesai, U. Lev, B. D. Bruner, O. Heber, and P. H. Bucksbaum, Phys. Rev. Lett. **116**, 143004 (2016).

[25] B. Feuerstein and U. Thumm, Phys. Rev. A **67**, 043405 (2003).

[26] R. Kosloff and H. Tal-ezer, Chem. Phys. Lett. **127**, 223 (1986).

[27] W. H. Press, S. A. Teukolsky, W. T. Vetterling, and B. P. Flannery, *Numerical Recipes: The Art of Scientific Computing*, 3rd ed. (Cambridge University Press, Cambridge, 2007), pp. 1048–1049.

[28] B. Feuerstein and U. Thumm, Phys. Rev. A **67**, 063408 (2003).

[29] T. E. Sharp, At. Data Nucl. Data Tables **2**, 119 (1970).

[30] See Supplemental Material at http://link.aps.org/supplemental/10.1103/PhysRevA.103.043122 for two movies showing the wave-packet propagation on the $2p\sigma_u$ state when the laser wavelengths are 400 and 800 nm.

[31] R. Numico, A. Keller, and O. Atabek, Phys. Rev. A **60**, 406 (1999).

[32] M. O. Scully and M. S. Zubairy, *Quantum Optics* (Cambridge University Press, Cambridge, 1997), pp. 151–154.

[33] A. S. Alnaser, X. M. Tong, T. Osipov, S. Voss, C. M. Maharjan, B. Shan, Z. Chang, and C. L. Cocke, Phys. Rev. A **70**, 023413 (2004).

[34] G. J. Halász, Á. Vibók, N. Moiseyev, and L. S. Cederbaum, Phys. Rev. A **88**, 043413 (2013).

[35] G. J. Halász, Á. Vibók, and L. S. Cederbaum, J. Phys. Chem. Lett. **6**, 348 (2015).